A&A 414, 1049–1063 (2004)
DOI: 10.1051/0004-6361:20031673

Astronomy & Astrophysics

Molecular and dust features of 29 SiC carbon AGB stars⋆

Xiaohong Yang, Peisheng Chen, and Jinhua He

National Astronomical Observatories/Yunnan Observatory, Chinese Academy of Sciences, PO Box 110, Kunming, 650011, PR China

Received 2 January 2003 / Accepted 8 October 2003

Abstract. We have reduced and analyzed the Infrared Space Observatory (ISO) Short-Wavelength Spectrometer (SWS) spectra of 29 infrared carbon stars with a silicon carbide feature at 11.30 μm, 17 of which have not been previously published. Absorption or emission features of C_2, HCN, C_2H_2, C_3 and silicon carbide (SiC) have been identified in all 17 unpublished carbon stars. In addition, two unidentified absorption features at 3.50 and 3.65 μm are listed for the first time in this paper. We classify these 29 carbon stars into groups *A*, *B*, *C* and *D* according to the shapes of their spectral energy distribution, and this classification seems to show an evolutionary sequence of carbon stars with an SiC feature. Moreover we have found the following results for the different groups: on average, the relative integrated flux of the 3.05 μm C_2H_2+HCN absorption feature increases gradually from group *A* to *B* and *C*; that of the 5.20 μm C_3 absorption feature becomes gradually weaker from group *A* to *B* and *C*; that of the 11.30 μm SiC emission feature increases gradually from group *A* to *B* and *C* but weakens in group *D*; and in contrast, that of the 13.70 μm C_2H_2 absorption feature weakens gradually from group *A* to *B* and *C* but becomes stronger in group *D*. We suggest that the evolution of the IR spectra of carbon stars along the sequence *A* to *D* is a result of the following phenomena: as the near-IR black-body temperature ($T_{\rm nir}$) decreases, the circumstellar envelope becomes thicker; also the effective temperature ($T_{\rm eff}$) of the photosphere of the central star decreases gradually and the C/O ratio increases from *A* to *B*.

Key words. star: carbon stars – star: AGB-infrared spectra-ISO

1. Introduction

Current theories in stellar evolution predict that stars with an initial mass of about 1 to 8 $M_\odot$ pass through two red-giant phases in the late stage of stellar evolution (Iben & Renzini 1983). The second red-giant phase is referred to as the Asymptotic Giant Branch (AGB) phase. This name originates from the fact that the temperature-luminosity (T-L) relationship for low-mass stars asymptotically approaches the T-L relationship for the stars on the first giant branch (Iben & Renzini 1983; Chan & Kwok 1988). In the AGB phase, the photospheric chemical abundances are changing due to the CNO process. Depending on the abundance ratio of C and O in the photosphere, the C/O ratio, the AGB stars are usually classified into oxygen-rich (M), S-type (S) and carbon-rich (C) stars (Iben & Renzini 1983). The M stars have C/O $\leq$ 0.6, the S stars C/O $\sim$ 0.8−1.0, and the C stars C/O $\sim$ 1.05−1.1 (Iben & Renzini 1983; Little-Marenin & Little 1988). As is generally known, and confirmed by observations (Wood 1985; Little-Marenin & Little 1988; Chen et al. 1990), some stars in the AGB phase evolve along the sequence M→S→C. For most of the AGB stars, the third dredge-up process in the He-shell carries carbon formed after helium burning onto the surface of stars, and the increase of the surface carbon abundance brings the surface C/O ratio from <1 to >1 and results in the formation of carbon stars (Iben & Renzini 1983).

Usually, carbon stars can be divided into three groups: visual carbon stars, infrared carbon stars (Chan & Kwok 1988, 1990; Bryan et al. 1990) and extreme carbon stars (Volk et al. 1992). The visual carbon stars whose mid-infrared spectra are mainly dominated by the photospheric continuum and that show a large excess at 60 μm, represent a transition phase which follows the interruption of mass loss from the oxygen-rich phase and begins a new phase of mass loss of carbon-rich material. The excess at 60 μm in these stars is due to the emission from the residual oxygen-rich material (Willems & de Jong 1988). The infrared carbon stars, whose infrared spectra are mainly due to the dust emission in the circumstellar envelope, are usually believed to be surrounded by a carbon-rich envelope characterized by the SiC emission feature at 11.3 μm (Chan & Kwok 1990). These stars are undergoing important mass loss and are likely to represent a more evolved phase of the stellar evolution than the visual carbon stars. The extreme carbon stars, whose derived mass loss rates and optical depths are both very high (Volk et al. 1992), are more evolved than the infrared carbon stars. These stars are expected to evolve into proto-planetary nebula (PPN) soon (Kwok 1993). The analysis presented in this paper is confined to the infrared carbon AGB stars (or SiC carbon stars) observed by ISO.

The chemical composition on the surface of an AGB star can be quite different for different C/O ratio, and therefore so

Send offprint requests to: Yang Xiaohong,
e-mail: ym990715@public.km.yn.cn

⋆ Based on observations with ISO, an ESA project with instruments funded by ESA Member States (especially the PI countries: France, Germany, The Netherlands and the UK) with the participation of ISAS and NASA.

will the chemical composition in the circumstellar envelope. These differences are reflected by the different infrared spectral features observed by ISO. Because the photospheric temperature of most AGB stars is less than 3000 K and most of their energy is radiated between 1 to 60 μm and the vibrational and rovibrational bands of many molecules also lie in this region, the study of infrared spectra in this wavelength range is very important to reveal the chemical composition of the circumstellar envelope, the dust formation process, and the evolutionary phase of the stars. At present, the identification of visual carbon stars is mainly based on the Swan system of C_2 bands (Chan 1992) in the optical region and a series of bands of CN and C_2 in the near infrared region. Nevertheless, the identification of infrared carbon stars is mainly based on the existence of carbide molecules, because most infrared carbon stars are obscured by a thicker circumstellar envelope and observing them in the optical region is very difficult. In the atmospheres of the carbon stars, oxygen atoms are tied up in the CO molecule and the rest of the carbon atoms often form carbides such as C_2, CN, CH, C_3, HCN, C_2H_2 and SiC. These molecules show absorption or emission features in the infrared spectra, and the relative intensities of the bands corresponding to these molecules put strict limits on the possible values of $T_{\rm eff}$, the gravity (specifically, Log G) and C/O (Jørgensen et al. 2000). In particular the ratio of the intensities in the 3 μm band (due to HCN and C_2H_2) and 5 μm band (due to CO and C_3) is a sensitive measure of the C/O ratio (Jørgensen et al. 2000).

ISO, developed by the European Space Agency and launched on 17 November 1995, provides us with a large amount of spectral data for the studying of molecules and dust features of AGB stars. Compared with the Infrared Astronomical satellite (IRAS), ISO is about 1000 times more sensitive and has about 100 times higher angular resolution. ISO made about 30 000 observations during its nearly 29 months lifetime, and 26 450 observations were made of astronomical objects ranging from solar system objects, stars to galaxies, in which many AGB stars were included.

In this paper we analyze the ISO SWS spectra of 29 carbon stars with an SiC feature at 11.30 μm, and 17 of these carbon-rich ISO sources are discussed for the first time. The 29 carbon stars are classified into four groups *A*, *B*, *C* and *D*. These different carbon stars are discussed in Sect. 1. Section 2 briefly describes the sample sources used in this paper. Different molecular features and the classification of these sample stars are discussed in detail in Sect. 3. Our main conclusions are presented in Sect. 4.

2. The SWS01 observations of 29 infrared carbon AGB stars

We have studied the infrared carbon AGB stars observed by the ISO SWS01 spectrometer. Infrared carbon AGB stars are characterized by the SiC spectral feature at 11.30 μm, and represent an important stage in the carbon star evolution between visual and extreme carbon stars (see introduction). Twenty-nine such sources are included in this paper. The ISO spectra of 12 of them have already been published in the literature; they are listed in Table 1. The ISO spectra of the remaining 17 sources have been reduced and analyzed for the first time for this paper; observational details are listed in Table 4.

We have reduced and analyzed the SWS01 spectra of all these 29 carbon stars, using the ISO Spectral Analysis Package (ISAP[1]). Some problems found during the data reduction are as follows: (1) ISAP does not provide tools for calibrating the memory effect of detectors. Small memory effects can be ignored and the average of up and down scans can be directly made. If the memory effect of one detector is prominent, all affected data of this detector can be deleted. In our samples, IRAS 18398-0220, IRAS 05028+0106, IRAS 06226-0905 and IRAS 02270-2619 show a memory effect in the 2A band (4.08−5.30 μm), and IRAS 03374+6229 and IRAS 21440+7324 also show it in the 2C band (7.0−12.0 μm); however the discrepancy between the up-scan and the down-scan is not more than ten percent so that the memory effect is neglected. (2) Another problem is the linking of different parts of the spectrum. For the absolute flux calibration of the different bands ("Lines" as put by ISAP) of the SWS01 spectrum, we use band 1A (2.38−2.60 μm) as the flux reference to calibrate the flux in the other bands. For the SWS01 observation, each pair of neighbouring bands has a small overlapping wavelength region. But actually, some spectra in our sources show a large discrepancy between two neighbouring bands in the overlapping region. There are two objects, IRAS 17419-1838 and IRAS 19248+0658, where one band shows a sharp jump in the overlapping region while the other band does not. In such a troublesome case, we simply link the two adjacent band strictly according to the effective wavelength range of each band. This problem does not affect our analysis of carbonaceous molecular features, but people who are interested in dust emission features should be aware of this problem.

The final reduced results are shown in Figs. 1 and 2. Many spectra are shown in the range 2.4−45.2 μm; however, most of spectra are affected by higher noise in the 25.0−45.2 μm region and these are only shown for 2.4−25.0 μm.

3. Discussion of ISO SWS features

ISO SWS01 spectral features of 29 infrared carbon AGB stars are presented in Figs. 1 and 2, for 20 objects the range is 2.4−25.0 μm and for 9 objects it is 2.4− 45.2 μm. The identified features are marked by letters as follows: "*a*" for C_2H_2+CO; "*b*" for HCN+ C_2; "*c*" for HCN+ C_2H_2; "*d*" for C_3; "*e*" for SiC and "*f*" for C_2H_2. Labels (such as "00172+4425") above the spectra are the IRAS names of the objects; labels (such as "(×1,+100)") below the spectra mean that spectra are first multiplied by a factor (such as "×1") and then shifted by adding an amount (such as "+100").

According to the Spectral Energy Distributions (SEDs) and some molecular features of the SWS spectra, these 29 carbon stars can be divided into 4 groups (see Figs. 1 and 2). **Group *A***: the intensity of the SEDs drops down towards longer wavelengths in the 2−15 μm range and becomes flatter after

[1] The ISO Spectral Analysis Package (ISAP) is a joint development by the LWS and SWS Instrument Teams and Data Centers. Contributing institutes are CESR, IAS, IPAC, MPE, RAL, and SRON.

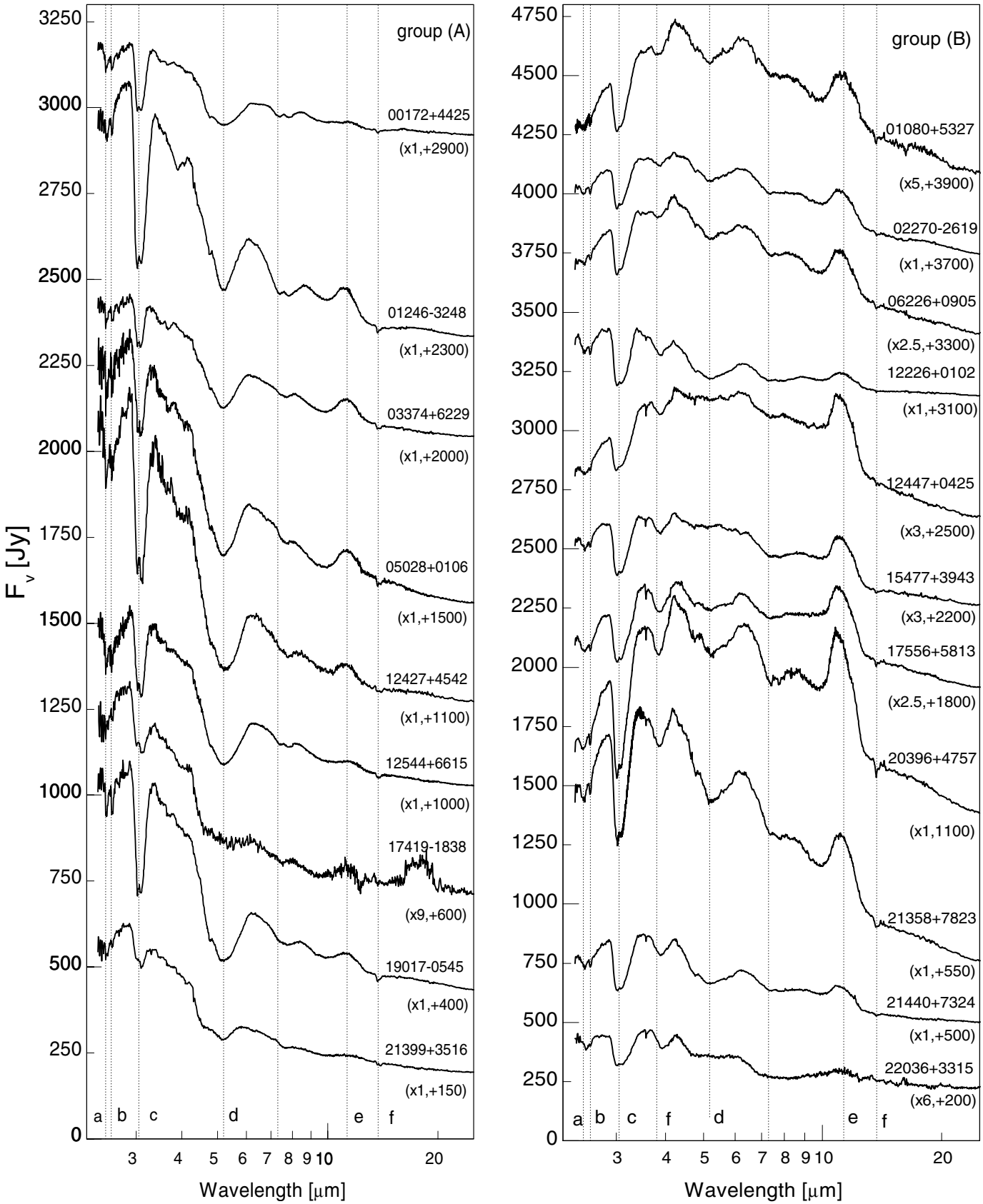

Fig. 1. ISO spectra are plotted in region of 2−25 μm for the 9 carbon stars (left panel) in group *A* and the 11 carbon stars (right panel) in group *B*. Different emission and absorption features are identified and marked by vertical lines and related letters. Marks in the figures are: "*a*" represents C_2H_2+CO; "*b*", HCN+ C_2; "*c*", HCN+ C_2H_2,; "*d*", C_3; "*e*", SiC and "*f*", C_2H_2. Labels (such as "00172+4425") above spectra are the IRAS name of the objects; labels (such as "(×1,+100)" below spectra mean that spectra are first multiplied by a factor (such as "×1") and then shifted by adding an amount (such as "+100").

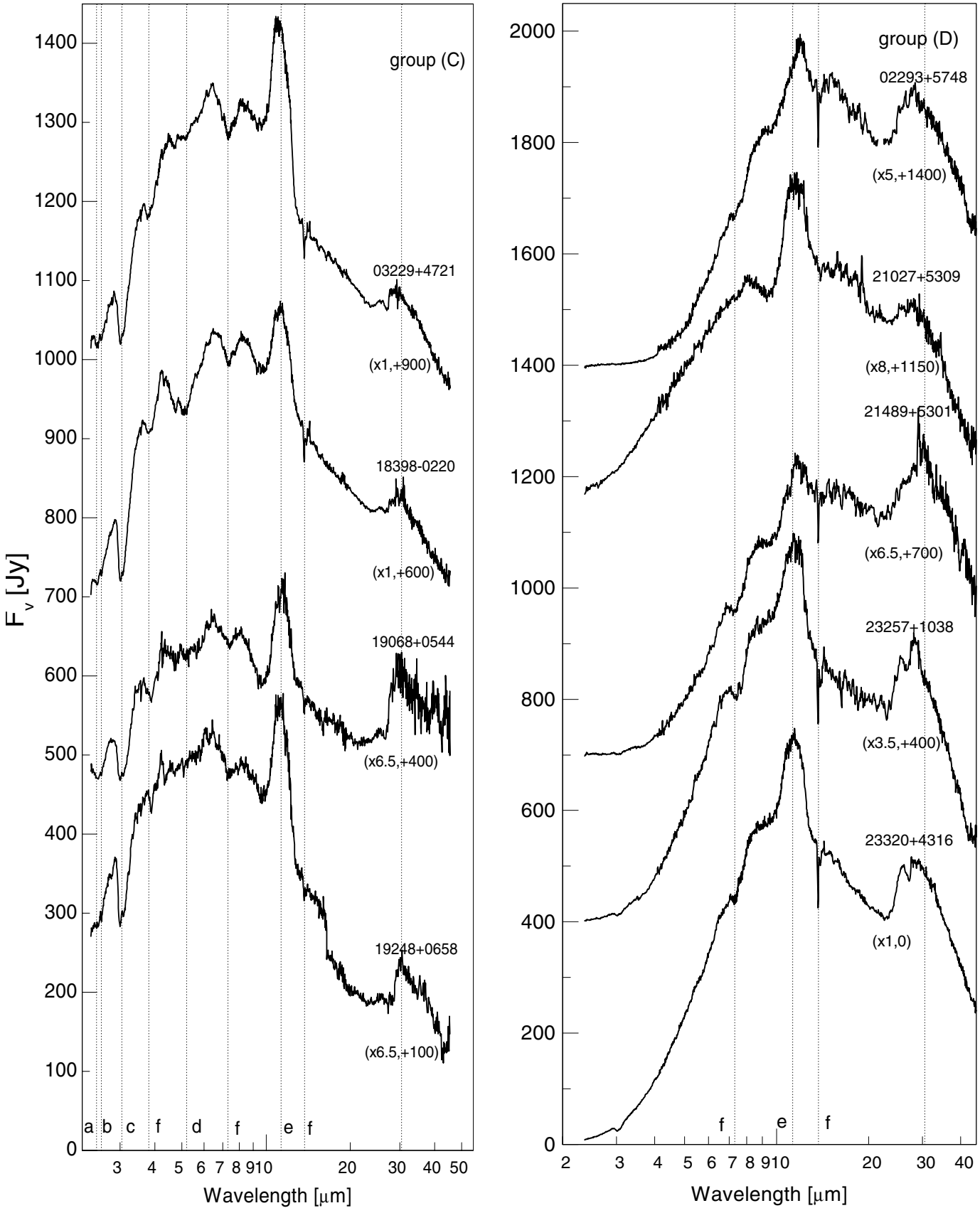

Fig. 2. ISO spectra are plotted for the region of 2−45 μm for the 4 carbon stars (left panel) in group *C* and the 5 carbon stars (right panel) in group *D*. Different emission and absorption features are identified and marked by vertical lines and letters. The marks and labels in this figure are the same as in Fig. 1.

Table 1. Published ISO SWS spectra of carbon stars with an SiC feature. The third column lists the features published in the literature listed in the last column.

IRAS	*Name*	*Spectral features* (*unit*: μm)	*References*
01246 − 3248	*R Scl*	2.48, 2.58, 3.05, 3.9, 5.20, 11.30, 13.70	(1), (2), (3)
02293 + 5748	*AFGL* 341	11.30, 13.7	(4)
12226 + 0102	*SS Vir*	2.48, 2.58, 3.05, 5.20, 11.30, 13.7	(4)
12447 + 0425	*RU Vir*	2.48, 2.58, 3.05, 3.9, 5.20, 11.30, 13.70	(2)
15477 + 3943	*V CrB*	3.05, 11.3, 13.7	(4)
17556 + 5813	*T Dra*	3.05, 11.3, 13.7	(5), (6)
19017 − 0545	*V Aql*	2.48, 2.58, 3.05, 5.20, 11.30, 13.70	(1)
20396 + 4757	*V Cyg*	2.48, 2.58, 3.05, 3.9, 5.20, 11.30, 13.70	(1)
21399 + 3516	*V*460 *Cyg*	3.50, 5.20, 11.3	(7), (8)
21489 + 5301	/	11.30, 13.70	(9)
22036 + 3315	*RZ Peg*	3.50, 3.56, 3.9, 11.30	(7)
23320 + 4316	*LP And*	3.05, 11.30, 13.70	(1)

(1) Yamamura et al. (1997); (2) Hron et al. (1997b); (3) Hron et al. (1998); (4) Aoki et al. (1999); (5) Hron et al. (1997a); (6) Loidl et al. (1997a); (7) Aoki et al. (1998); (8) Jørgensen et al. (2000); (9) Volk et al. (2000).

Table 2. The classification of all 29 sources and spectral features found for each group.

Classification	*Main spectral features* *Unit*: μm	*Sources* (*IRAS*)
A	2.48, 2.58, 3.05, 5.20, 11.30, 13.70	00172 + 4425, 01246 − 3248*, 03374 + 6229, 05028 + 0106, 12427 + 4542#, 12544 + 6615, 17419 − 1838#, 19017 − 0545*, 21399 + 3516*
B	2.48, 2.58, 3.05, 3.56, 3.90, 5.20, 11.30, 13.70	01080 + 5327, 02270 − 2619, 06226 − 0905, 12226 + 0102*, 12447 + 0425*, 15477 + 3943*, 17556 + 5813*, 20396 + 4757*, 21358 + 7823, 21440 + 7324, 22036 + 3315*#
C	2.48, 2.58, 3.05, 3.56, 3.90, 5.20, 7.30, 11.30, 13.70	03229 + 4721, 18398 − 0220, 19068 + 0544, 19248 + 0658+
D	11.30, 13.70	02293 + 5748*, 21027 + 5309, 21489 + 5301*, 23257 + 1038, 23320 + 4316*

Notes: a) "*" means that the ISO SWS result is already published; b) "#" means that the objects do not show the 13.7 μm C_2H_2 feature; c) "+" means that the object does not show the 5.20 μm C_3 feature.

15 μm; for the 3.05 μm absorption feature, the intensity of the left wing is usually higher than that of the right wing. **Group *B***: the intensity of the SEDs first rises towards longer wavelengths in the 3−4 μm range, then drops down in the 4−15 μm range and becomes flatter after 15 μm. For the 3.05 μm feature, the intensity of the left wing is usually lower than that of the right wing. **Group *C***: the intensity of the SEDs rises towards longer wavelengths in the range shorter than about 7 μm and drops in the 7−25 μm region. SEDs in this group are usually complicated due to more molecular absorption and emission features. In addition, SEDs show a wide bump peaking at around 30 μm. **Group *D***: the energy flux is nearly zero in the near-infrared region, and spectral shapes show obvious double peaks in the 2−45 μm region. The classification of the 29 carbon stars and spectral features for each group are given in Table 2. It can be seen that the main infrared features of the different groups are quite different, for example the 3.90 and 3.56 μm absorption features only appear in groups *B* and *C*.

Some detailed information for all 29 objects is given in Table 3 in which: Col. 1 is the classification of carbon stars given in this paper; Col. 2 IRAS name, where ISO SWS spectra of sources marked by "*" have been published; Cols. 3−4, 6−7, 8−9, 11−12, 16, and 18−19 give the relative integrated flux of 2.48+2.58, 3.05, 3.50+3.65, 3.56, 3.90, 5.20, 7.30, 11.30, 13.7, 14.04 and 14.30 μm features respectively. The relative integrated flux is defined as the ratio of the quantity derived by the subtraction of the integrated continuum flux from the integrated line flux, and the integrated continuum flux. Although the line widths of the different objects for the same line feature are different, we integrate over the same fixed wavelength range for each line feature to derive its integrated flux. The integration ranges are: 2.40−2.76 μm for 2.48+2.58 μm

Table 3. Derived and cited data of the carbon stars in groups *A*, *B*, *C* and *D*.

(1) groups	(2) samples	(3) 2.48 (+2.58)	(4) 3.05	(5) $D_{3.05}$	(6) 3.50 (+3.65)	(7) 3.56	(8) 3.90	(9) 5.20	(10) $D_{5.20}$	(11) 7.30	(12) 11.30	(13) $H_{11.30}$	(14) $\lambda_{11.30}$	(15) Dust	(16) 13.70	(17) $D_{13.70}$	(18) 14.04	(19) 14.30	(20) *CV*	(21) T_{eff}	(22) T_{nir}
	00172 + 4425	0.119	0.216	0.678	0.047	/	/	0.338	0.672	?	0.089	0.277	11.46	SiC_{++}	0.086	0.225	/	0.004	$CV6$	2455	2300
	01246 − 3248*	0.030	0.278	0.689	/	/	0.047	0.251	0.583	?	0.224	0.747	11.31	SiC_{++}	0.102	0.311	/	0.012	$CV4$	2625	2590
	03374 + 6229	0.062	0.077	0.443	0.044	/	/	0.213	0.514	?	0.184	0.573	11.34	SiC_{+}	0.074	0.188	/	0.007	$CV4$	2695	2070
A	05028 + 0106	0.069	0.090	0.297	0.043	/	/	0.248	0.549	?	0.139	0.421	11.34	SiC_{+}	0.071	0.189	/	0.005	$CV5$	2625	2610
	12427 + 4542	0.103	0.194	0.437	/	/	/	0.251	0.502	?	0.077	0.278	11.57	SiC_{+}	/	/	/	/	$CV5$	2810	2650
	12544 + 6615	0.156	0.138	0.476	0.034	/	/	0.341	0.683	?	0.094	0.206	11.35	SiC_{+}	0.088	0.192	/	/	$CV5$	2760	2640
	17419 − 1838	0.062	0.098	0.221	/	/	/	0.169	0.295	?	0.161	0.420	11.30	/	/	/	/	/	$CV1$	3220	2830
	19017 − 0545*	0.147	0.193	0.547	0.021	/	/	0.330	0.667	?	0.118	0.367	11.38	SiC_{+}	0.092	0.239	/	0.010	/	/	2920
	21399 + 3516*	0.034	0.072	0.206	/	/	/	0.183	0.374	?	0.053	0.145	11.49	SiC_{+}	0.053	0.104	/	/	$CV2$	2950	2680
	01080 + 5327	0.060	0.198	0.397	/	/	0.042	0.096	0.209	?	0.143	0.414	11.36	SiC	0.026	0.112	/	0.036	/	/	1010
	02270 − 2619	0.059	0.177	0.433	/	/	0.047	0.094	0.218	?	0.183	0.558	11.34	SiC	0.030	0.097	0.015	0.018	$CV7$	2060	1250
	06226 − 0905	0.030	0.148	0.375	/	/	0.033	0.109	0.223	?	0.179	0.522	11.29	SiC_{+}	0.030	0.095	0.003	0.015	/	/	1220
	12226 + 0102*	0.148	0.329	0.729	/	0.013	0.119	0.254	0.491	?	0.177	0.544	11.31	$Br1$	0.022	0.120	/	/	$CV6$	2560	1680
	12447 + 0425*	0.051	0.178	0.341	/	0.026	0.061	0.067	0.112	?	0.251	0.640	11.22	SiC	0.017	0.075	/	/	/	/	1050
B	15477 + 3943*	0.066	0.233	0.539	/	0.020	0.081	0.038	0.108	?	0.264	0.798	11.30	SiC	0.032	0.103	/	0.019	$CV7$	2090	1260
	17556 + 5813*	0.137	0.255	0.523	/	0.033	0.094	0.114	0.220	?	0.337	0.721	11.16	SiC	0.027	0.123	0.006	0.020	/	/	1160
	20396 + 4757*	0.064	0.212	0.526	/	/	0.080	0.098	0.195	?	0.225	0.573	11.23	SiC	0.033	0.129	/	0.015	/	/	1080
	21358 + 7823	0.042	0.178	0.423	/	0.005	0.056	0.108	0.239	?	0.153	0.467	11.30	SiC_{+}	0.032	0.087	0.010	0.009	$CV6$	2095	1360
	21440 + 7324	0.096	0.284	0.623	/	0.018	0.104	0.213	0.427	?	0.292	0.920	11.34	SiC_{+}	0.109	0.289	/	/	/	/	1670
	22036 + 3315*	0.077	0.293	0.541	/	0.045	0.128	0.127	0.255	?	0.123	0.305	11.07	/	/	/	/	/	$CV5$	2605	1600
	03229 + 4721	0.069	0.169	0.425	/	0.015	0.057	0.050	0.103	0.065	0.232	0.614	11.30	SiC	0.033	0.151	/	0.021	$CV7$	1820	850
C	18398 − 0220	0.066	0.188	0.461	/	0.011	0.051	0.109	0.213	0.036	0.112	0.320	11.34	/	0.028	0.134	0.010	0.021	/	/	860
	19068 + 0544	0.122	0.271	0.539	/	0.045	0.125	0.092	0.155	0.051	0.216	0.672	11.36	/	0.044	0.154	/	/	/	/	890
	19248 + 0658	0.034	0.149	0.350	/	0.024	0.014	/	/	0.048	0.210	0.616	11.35	/	0.031	0.112	0.008	0.006	/	/	1080
	02293 + 5748*	/	/	/	/	/	/	/	/	/	0.057	0.158	11.76	/	0.054	0.229	/	0.006	/	/	370
	21027 + 5309	/	/	/	/	/	/	/	/	/	0.221	0.539	11.50	/	0.022	0.077	/	0.001	/	/	630
D	21489 + 5301*	/	/	/	/	/	/	/	/	0.048	0.026	0.109	11.74	/	0.034	0.196	/	/	/	/	400
	23257 + 1038	/	/	/	/	/	/	/	/	0.044	0.127	0.302	11.47	/	0.074	0.257	/	0.018	/	/	470
	23320 + 4316*	/	/	/	/	/	/	/	/	0.021	0.110	0.292	11.42	*red*	0.038	0.208	/	0.009	/	/	520

Col.1 is the classification of carbon stars given in this paper; col. 2 IRAS name, where ISO SWS spectra of samples marked by '*' have been published; cols. 3−4, 6−7, 8−9, 11−12, 16 and 18−19 give the relative integrated flux of the 2.48+2.58, 3.05, 3.50+3.65, 3.56, 3.90, 5.20, 7.30, 11.30, 13.7, 14.04 and 14.30μm features respectively; cols. 5, 10, 13 and 17 are the normalized line center depth or normalized line peak height of 3.05, 5.20, 11.30 and 13.70μm features respectively; col. 14 the peak wavelength of the 11.3μm features in μm ; col. 15 classification of SiC dust (Sloan et al. 1998). cols. 20−21 the classification and T_{eff} given by Bergeat et al. (2001) in [K]; col. 22 T_{nir} of samples in [K], which is derived by single-blackbody fitting of the 2.3-11.0μm range. In col. 11 '?' means that the identification of this feature is still controversial.

features, 2.85−3.50 μm for the 3.05 μm feature, 3.35−3.80 μm for 3.50+3.65 μm features, 3.54−3.62 μm for 3.56 μm feature, 3.60−4.20 μm for the 3.90 μm feature, 4.10−6.50 μm for the 5.20 μm feature, 6.40−8.20 for the 7.30 μm feature, 9.00−13.60 μm for the 11.30 μm feature, 13.40−14.30 μm for the 13.7 μm feature, 14.00−14.15 μm for the 14.04 μm feature and 14.20−14.43 μm for the 14.30 μm feature. The 2.48 and 2.58 μm absorption features are considered to be a combined feature because they are always found to be partly overlapped. The same applies to the combined 3.50 and 3.65 μm features. In Col. 11, the mark "?" means that identification of this feature is still controversial. The errors in the derived quantities in Table 3 mainly originate from three sources: the ISO sensitivity limit, which causes a relative error usually lower than one percent in the 2.4−25 μm region and which does not include the error due to the memory effect and the error caused by processing the data; fitting of the continuum of these different molecular and dust features by polynomial formulae, which results in an uncertainty of at most ten percent; the partial overlapping of neighboring features, which causes large errors of fitting of the continuum of these different molecular features. As the SWS01 spectrum begins at 2.38 μm, it is difficult to determine the accurate continuum baseline for the 2.48+2.58 μm features, and therefore the calculated values may be lower limits. Columns 5, 10, 13 and 17 are the normalized line center depths or line peak heights of the 3.05, 5.20, 11.30 and 13.70 μm features respectively. The normalized line center depth (D) or line peak height (H) is defined as the flux of the center of the line divided by the flux of the center of the line continuum. Column 14 is the peak wavelength of the 11.3 μm feature in μm. Note that the relative integrated flux of the 13.7 μm feature is calculated after removing the 14.03 and 14.30 μm emission features from its red wing, and that the normalized line peak height in Col. 13 and the actual peak wavelength in Col. 14 for the 11.3 μm feature are derived by fitting a Gaussian profile. Column 15 is the classification of SiC dust given by Sloan et al. (1998); Cols. 20−21 are the photometrical classification and $T_{\rm eff}$ given by Bergeat et al. (2001) in [K]; Col. 22 is $T_{\rm nir}$ of the sources in [K], which is obtained by single-blackbody fitting for the 2.3−11.0 μm range.

The different identified features in the ISO SWS01 spectra of the 29 carbon stars, in Figs. 1 and 2, are caused by the different vibrational bands of molecules. Based on the spectra of some carbon stars already published, various features in the spectra of the 17 unpublished carbon stars were identified: the 2.48 μm feature is due to C_2H_2(10001) and CO($\Delta\nu = 2$); the 2.58 μm feature to HCN(011) and $C_2(\Delta\nu = -1)$; the 3.05 μm feature to HCN(001) and C_2H_2(01011+00100); the 3.56 μm feature to HCN(110); the 3.90 μm feature to C_2H_2(01001); the 5.20 μm feature to C_3(001) (Hron et al. 1997a); the 7.30 μm feature to C_2H_2 (00011); the 11.30 μm feature to SiC and the 13.70 μm feature to C_2H_2(00001) (Aoki et al. 1999). Special attention should be given to two absorption features at 3.50 μm and 3.65 μm; although these have not been reported previously they do appear in the spectra of five sources in group *A* (IRAS 00172+4425, IRAS 03374+6229, IRAS 05028+0106, IRAS 12544+6615 and IRAS 19017-0545). Figure 3 shows these two features in more details. Although they seem to be very faint, their simultaneous appearance in the five sources and the similarities of their spectral profile, combined with the fact that they do not appear in other studied spectra, prove that the two features cannot be caused by instrumental effects but are actually unknown molecular absorption features.

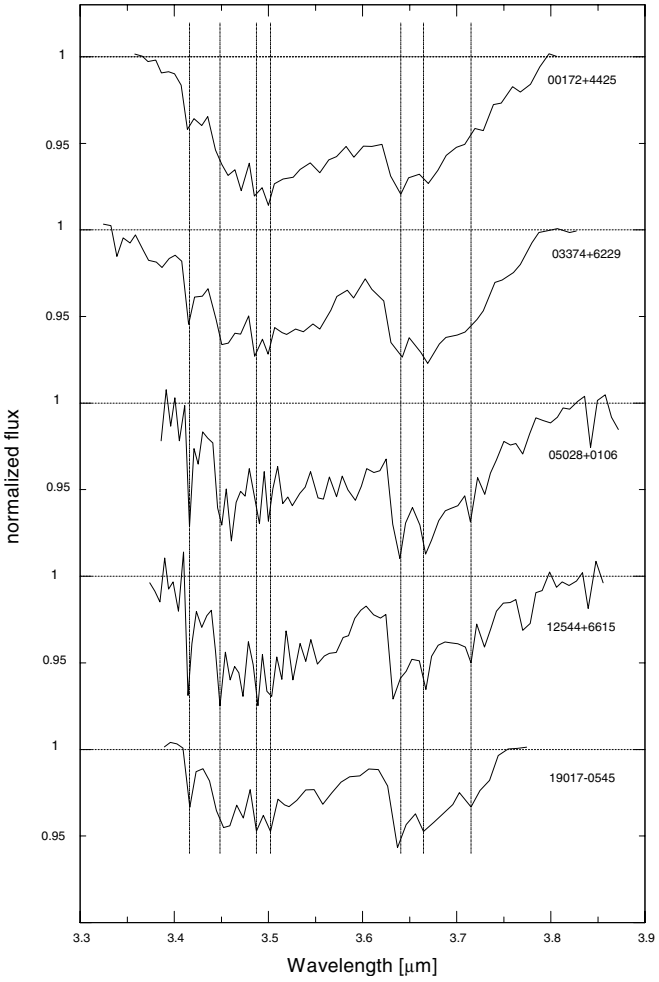

Fig. 3. Diagram of the normalized spectral profiles for the two unidentified absorption features (the 3.50 and 3.65 μm features) found in the five objects of group *A*.

What is the relation between the four groups defined in this paper? Do carbon stars in groups *A*, *B*, *C* and *D* respectively represent different evolutionary stages? We can try to find answers from the data in Table 3. In fact, the sequence $A \rightarrow B \rightarrow C \rightarrow D$ is also the sequence of decreasing $T_{\rm nir}$. For group *A*, nearly all $T_{\rm nir}$ are between 2600 K and 3000 K except IRAS 03374+6229 with 2070 K, and all $T_{\rm eff}$ are between 2400 K and 3300 K, but for every object $T_{\rm nir}$ is lower than $T_{\rm eff}$; for group *B*, $T_{\rm nir}$ is between 1000 K and 1700 K and $T_{\rm eff}$ is mainly near to 2100 K; for group *C*, $T_{\rm nir}$ is between 800 K and 1100 K; for group *D*, $T_{\rm nir}$ is between 300 K and 700 K.

Bergeat et al. (2001) have shown that the decrease of $T_{\rm eff}$ in carbon-rich stars is tightly correlated with the increase of j in the photometrical classification $\rm CV_{\it j}$ for carbon stars. In this classification SEDs are classified into 14 photometric groups ($\rm HC_{\it i}$, $\rm CV_{\it j}$ and SCV with $i = 0, 5$ and $j = 1, 7$); the $\rm CV_{\it j}$ classification applies to the cool carbon (CV) variables, and is

correlated with the increase of the C/O ratio in the photosphere. Combining this conclusion with our classification results, we deduce that going from *A* to *B* $T_{\rm eff}$ decreases and the C/O ratio shows a gradual increase.

Figures 1 and 2 and the comments made above on the classification of the SEDs clearly show that, from group *A* to *B* to *C* to *D*, the maximum flux of the near-infrared continuum shifts gradually towards longer wavelengths, and the mid-infrared bump peaking at about 30 μm develops gradually, eventually reaching a considerable height in group-*D* sources. This means that the emitting circumstellar dust envelope becomes colder and more massive along the sequence $A \rightarrow B \rightarrow C \rightarrow D$.

All figures from Figs. 5 to 16 (visualizing the data in Table 3) show the relation of the relative integrated flux of different features among different classification types. The following conclusions can be reached from these figures: (1) from group *A* to *B* and *C*, the relative integrated flux of the 3.05 μm C_2H_2+HCN absorption and 11.30 μm SiC emission is gradually enhanced while that of the 5.20 μm C_3 and 13.70 μm C_2H_2 absorptions is gradually weakened; (2) from group *B* to *C*, no systematic difference can be found for any of the four line features (the 3.05, 5.20, 11.30, 13.70 μm features); (3) in group *D*, the 3.05 and 5.20 μm features become very faint or disappear completely while in this group on the whole the 11.3 μm emission is weaker and the 13.7 μm absorption is stronger than in groups *B* and *C*. These variations of the molecular band features may indicate the evolution of the molecular content of the carbon star photosphere.

3.1. Properties of the various features in the four groups

3.1.1. Comparing group *A* with groups *B*+*C* in the 3–4 μm region

There are many molecular absorption features in the 3−4 μm region. The features originate from outside the stellar photosphere, and thus they can reflect physical and chemical characteristics of the region between the stellar photosphere and the inner circumstellar envelope. After comparing the SWS01 spectra of groups *A* and *B*+*C*, we find the following: (1) the relative integrated flux of the 3.05 μm C_2H_2+HCN absorption is gradually increased from *A* to *B*+*C*. This is shown in Fig. 5, which is a diagram of the relative integrated flux against $T_{\rm nir}$ for the 3.05 μm absorption feature. (2) The 3.05 μm absorption feature is broader in groups *B* and *C* than in group *A*, and the difference mainly appears in the red wing of the absorption feature, as can be seen from Fig. 4, which shows normalized ISO spectra of 25 objects around 3.05 μm. This point is also illustrated in Fig. 6 in which the relative integrated flux is shown against the normalized line center depth for the 3.05 μm absorption feature. We have fitted a line (the solid line in the figure) for all points in Fig. 6 and this line naturally acts as a line dividing the group-*A* sources from the other two groups. Since the relative integrated flux of the 3.05 μm feature coming from the objects of groups *B* and *C* is higher than that observed for group *A*, with the same normalized line center depth, this separation into two halves

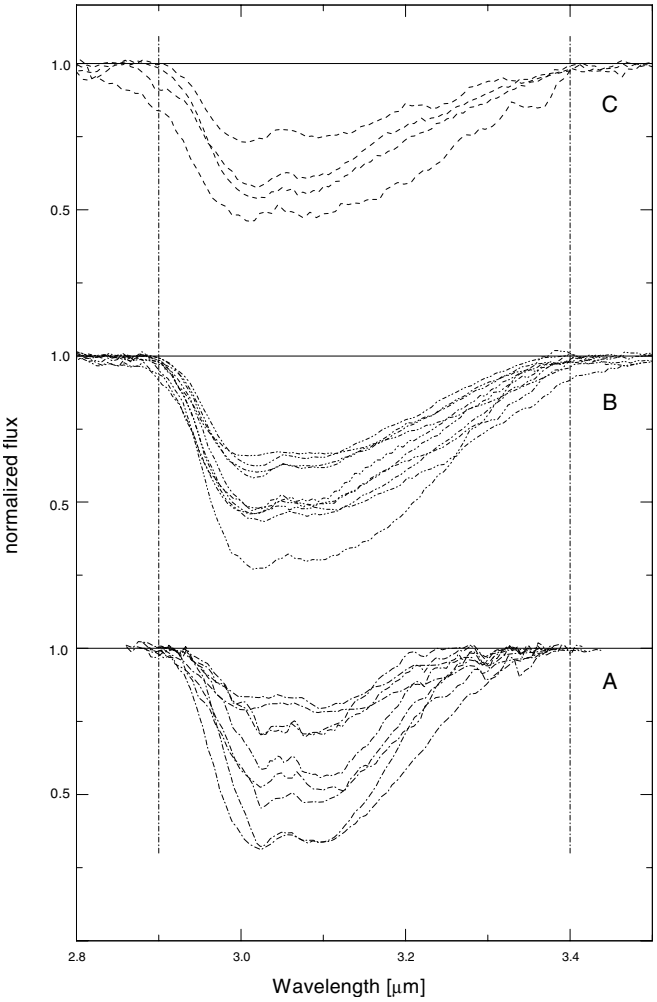

Fig. 4. Normalized spectral profiles of the 3.05 μm C_2H_2+HCN absorption feature for 25 objects. They are grouped in three panels according to our classification for comparison.

qualitatively confirms the conclusion that the 3.05 μm feature is broader in groups *B* and *C* than in group *A*. (3) Several group-*A* sources show two unidentified absorption features at 3.50 and 3.65 μm (see the profiles shown in Fig. 3) which are found for the first time in this paper, while no group -*B* and -*C* sources show them. (4) Most group -*B* and -*C* sources show 3.9 μm C_2H_2 absorption, but no group-*A* sources do, with one exception, viz. IRAS 01246-3248. (5) Some group-*B* sources and all group-*C* sources show 3.56 μm HCN absorption, but none of the group-*A* sources does. Yamamura et al. (1997) performed a similar analysis for their ten carbon stars and divided them into four groups according to their near-infrared color temperatures. All sources in their groups II and III are completely included in our groups *A* and *B* respectively. Our conclusions (2) and (4) confirm the conclusions of Yamamura et al. (1997). This agreement between our classification and theirs is reasonable because the shape of the infrared SED used as criterion in our classification is approximately equivalent to near-infrared color temperature. However, the origin of this difference between group *A* and *B* (or group II and III of Yamamura et al.) is still unclear. As Yamamura et al. (1997)

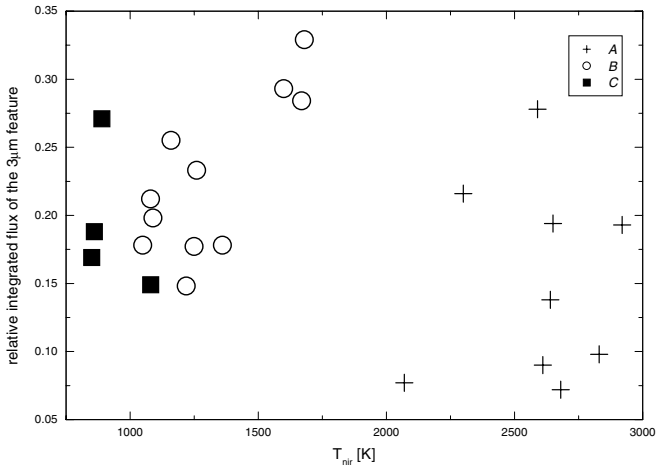

Fig. 5. Diagram of the relative integrated flux against $T_{\rm nir}$ for the 3 μm C_2H_2+HCN feature. Group-*A* sources are represented by a cross; group-*B* sources by a circle; group-*C* sources by a square.

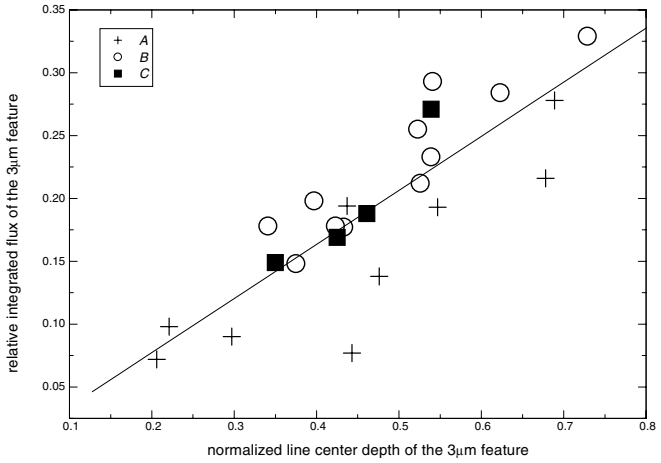

Fig. 6. Diagram of the relative integrated flux against the normalized line center depth for the 3 μm C_2H_2+HCN feature. Group-*A* sources are represented by a cross; group-*B* sources by a circle; group-*C* sources by a square.

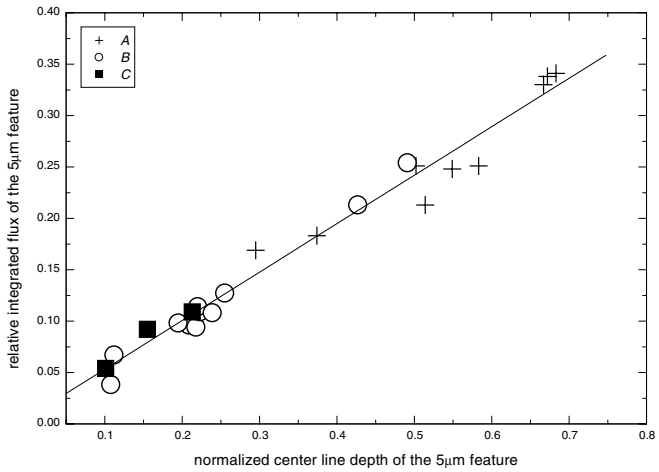

Fig. 7. Diagram of the relative integrated flux against the normalized line center depth for the 5 μm C_3 feature. Group-*A* sources are represented by a cross; group-*B* sources by a circle; group-*C* sources by a square.

put it, this difference may be caused by the difference in the structure of the extended hot molecular layer outside the photosphere, i.e. there is a quasi-static region between the atmosphere and the circumstellar envelope for group *B* (Tsuji et al. 1997). The numeric computation performed by Loidl et al. (1997b) showed that the broadening of the 3.05 μm feature and the 3.90 μm feature could be the result of the strengthening of hot bands of C_2H_2 originating in an extended molecular layer with temperature between 1000 K and 1500 K.

3.1.2. The 5.20 μm C_3 feature

The absorption feature centered at about 5.20 μm is due to C_3(001). Since C_3 was detected in a cometary tail in the 18th century, and Douglas (1951) identified it in the laboratory, it has been realized that C_3 plays an important role in astrophysics, such as for the formation of carbon-chains (Cernicharo et al. 2000). The molecule C_3 in the atmosphere of cool stars was detected in the optical bands (Zuckerman et al. 1976), and recent work on ISO spectra indicated that C_3 is very abundant in carbon stars. The formation of C_3 requires a combination of relatively high partial pressure and low temperature. Its main spectral feature is the fundamental C-C stretching at 5.20 μm which forms in an environment of about 2000 K (Loidl et al. 1999). Figures 8 and 7 show the relative integrated flux of the 5.20 μm feature against $T_{\rm nir}$ and the normalized line center depth respectively. A straight line is fitted to all points in Fig. 7. This linear correlation implies that the basic profiles of this feature do not vary essentially from group *A* to *B*+*C*, except in their intensities. The relative integrated flux in Fig. 8 decreases with decreasing $T_{\rm nir}$ along the *A*→*B*+*C* sequence and becomes undetectable in group-*D* sources. This declining tendency of the 5.20 μm C_3 feature can be explained directly by the decrease of $T_{\rm eff}$ and the increase of the optical depth in the circumstellar envelope along the same sequence, as follows: the 5.20 μm C_3 feature is generally generated in the stellar photosphere and atmosphere, and the temperature of the stellar photosphere affects the amount of C_3. On the other hand, this 5.20 μm C_3 feature disappears in group *D*, which may be due to the very high optical depth in the circumstellar envelope, because it is not all certain that $T_{\rm eff}$ of group-*D* sources is lower than that of group-*C* sources (see second paragraph in Sect. 3.1.5), and then the very high optical depth in the circumstellar envelope may explain the disappearance of the feature in group *D*. However, it is difficult to disentangle the contributions of $T_{\rm eff}$ (of the stellar photosphere) and of the optical depth (in the circumstellar envelope) to the 5.20 μm C_3 feature, because the definite $T_{\rm eff}$ of group-*D* sources cannot be obtained.

The intensity ratio of the 3 μm band (due to HCN and C_2H_2) and 5 μm band (due to CO and C_3) is a sensitive measure of the C/O ratio (Jørgensen et al. 2000). To emphasize this point, we show Fig. 9, a diagram of the relative integrated flux ratio of the 3.05 and 5.20 μm features (abbreviated as 3.05 μm/5.20 μm) against $T_{\rm nir}$. From this figure, we reach the qualitative conclusion that this 3.05 μm/5.20 μm ratio increases from *A* to *B*+*C*. On the other hand, we have earlier reached the

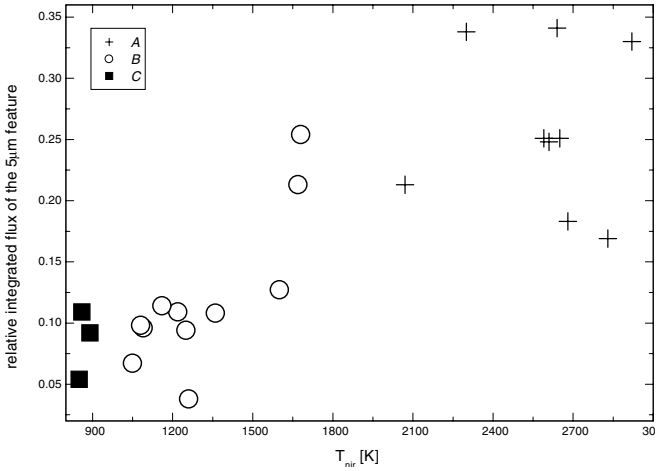

Fig. 8. Diagram of the relative integrated flux against $T_{\rm nir}$ for the 5 μm C_3 feature. Group-*A* sources are represented by a cross; group-*B* sources by a circle; group-*C* sources by a square.

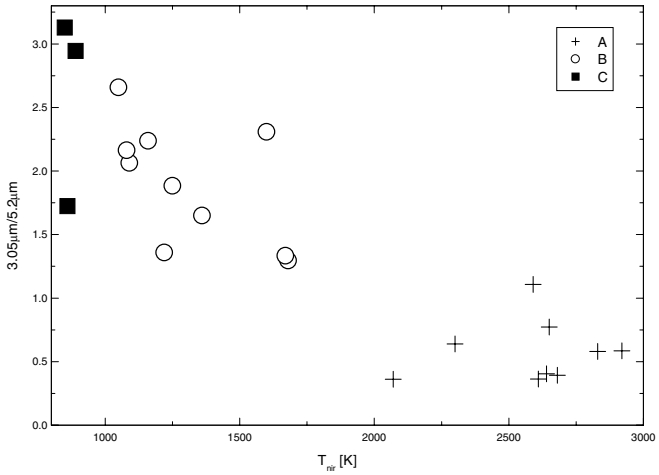

Fig. 9. Diagram of the relative integrated flux ratio of the 3.05 and 5.20 μm feature against $T_{\rm nir}$. Group-*A* sources are represented by a cross; group-*B* sources by a circle; group-*C* sources by a square.

conclusion that the C/O ratio increases from *A* to *B*. Therefore, we suggest that the increase of 3.05 μm/5.20 μm could be tracing an increase of the C/O ratio.

3.1.3. 6−9 μm range

The 6−9 μm spectra of carbon stars have been discussed by many authors (Willems 1988a; 1988b; Hron et al. 1998; Aoki et al. 1999). Willems (1988b) thought that the material producing the 8.6 μm feature forms under the same physical and chemical conditions as HCN and C_2H_2, either together with HCN and C_2H_2 or as a result of reactions of HCN and C_2H_2. On the other hand, Hron et al. (1998) and Aoki et al. (1999) thought that the 8.6 μm feature originates from the interaction of the 7.5 μm absorption and the 11.3 μm emission. In our sources, the 7.3 μm absorption seems more like the end of the blue wing of 8.6 μm emission in groups *A* and *B* and more like molecular absorption in groups *C* and *D*. We also suggest that $C_2H_2(\nu_4+\nu_5)$ (and HCN) and SiC jointly determine the spectral shape between 6−9 μm. However, when the SiC dust feature changes from group *A* to *B* to *C* to *D* (see Sect. 3.1.4), the $C_2H_2(\nu_4+\nu_5)$ absorption shows more clearly. Note that the line center wavelength of the 7.3 μm feature is not exactly at 7.5 μm, the theoretical position of $C_2H_2(\nu_4+\nu_5)$ absorption band.

3.1.4. The 11.30 μm SiC feature

The diagram of peak wavelength against the relative integrated flux for 11.30 μm SiC emission is shown in Fig. 10. This figure indicates that the relative integrated flux of the 11.30 μm SiC feature is higher in groups *B* and *C* than in groups *A* and *D*. This can be explained as an optical depth effect: Group-*B* sources are generally optically thicker than group-*A* sources, so the 11.30 μm SiC emission is stronger in the former; the optical depth of group-*D* sources probably becomes so high that only their outer SiC regions, which are the coolest, can be detected, resulting in a weaker emission of the SiC feature. On the other hand, it can be seen from this figure

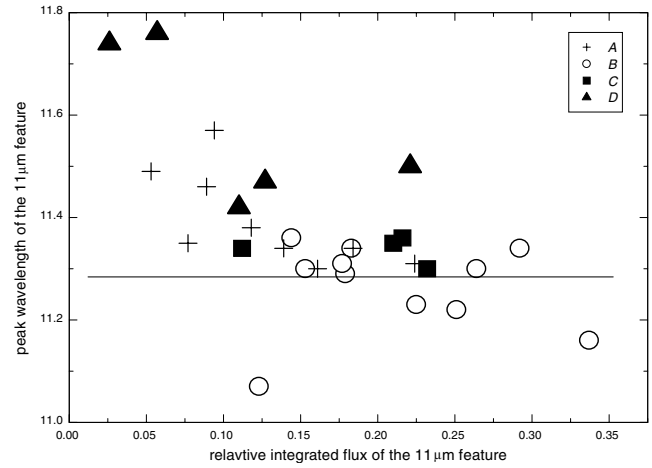

Fig. 10. Diagram of the peak wavelength against the relative integrated flux for the 11 μm SiC feature. Group-*A* sources are represented by a cross; group-*B* sources by a circle; group-*C* sources by a square; group-*D* sources by a triangle.

that the actual peak wavelength of the 11.30 μm SiC feature varies among different sources in different groups. The sources with the strongest SiC emission (groups *B* and *C*) peak at bluer wavelengths. As we have discussed above, $T_{\rm nir}$ of the sources in groups *A* and *D* is respectively highest and lowest among the four groups. This implies that this behavior of the SiC 11.30 μm emission feature can not be explained only by a difference in the $T_{\rm nir}$, i.e. in the increasing and cooler circumstellar dust envelope. For a satisfying explanation, the difference in the structure and/or composition of the SiC dust should be considered.

In Fig. 11, the different lines are derived by fitting data of different groups, and the relative integrated flux of the 11.30 μm feature is found to be approximately linearly correlated with the normalized line peak height for all the objects, as expected. This linear correlation may imply that the shapes of the emission feature are similar in the objects of the different groups with quite different optical depth. But with a closer inspection, we find three points worthy to be noted: 1) the linear

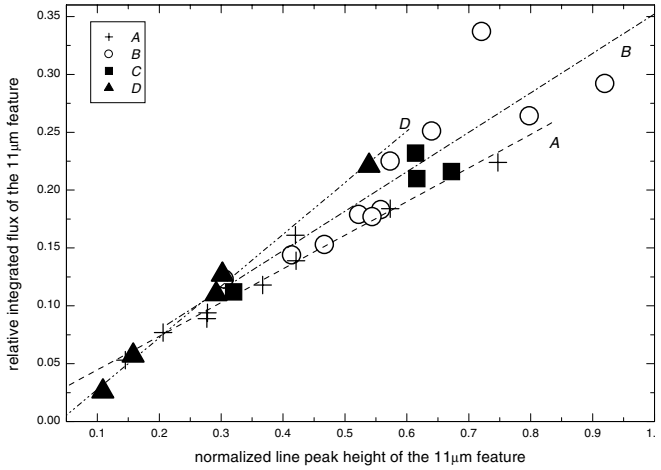

Fig. 11. Diagram of the relative integrated flux against the normalized line peak height for the 11 μm SiC feature. Different lines are derived by fitting data of different groups respectively. Group-*A* sources are represented by a cross; group-*B* sources by a circle; group-*C* sources by a square; group-*D* sources by a triangle.

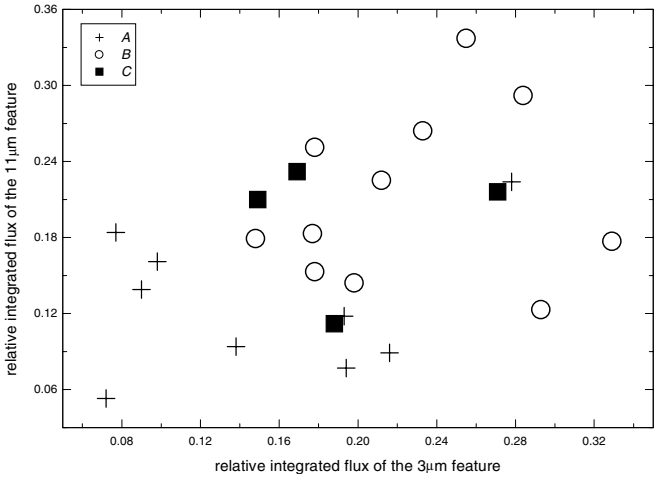

Fig. 12. Diagram of the relative integrated flux of 11 μm SiC feature against that of the 3.05 μm C_2H_2+HCN feature. Group-*A* sources are represented by a cross; group-*B* sources by a circle; group-*C* sources by a square.

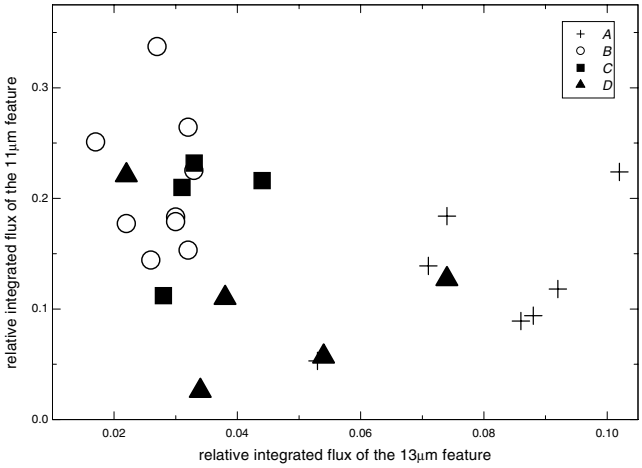

Fig. 13. Diagram of the relative integrated flux of 11 μm SiC feature against that of the 13.70 μm C_2H_2 feature. Group-*A* sources are represented by a cross; group-*B* sources by a circle; group-*C* sources by a square; group-*D* sources by a triangle.

correlation is better for individual groups than for all the objects. The correlation is best in groups *A* and *D*, and worst in groups *C* and *B*. 2) The slope of the linear correlation becomes steeper from group *A* to *B* to *D*. 3) Group-*C* sources are distributed around the line for group-*B* data. Therefore, the profiles of the SiC feature are uniform for objects in one and the same group, and vary in a regular manner from group *A* to *B*+*C* to *D*.

Column 15 of Table 3 gives another SiC feature classification system given by Sloan et al. (1998) for most of our samples. They divided carbon-rich emission into six types: red, SiC, SiC+, SiC++, Broad1 and Broad2. In their classification, from SiC++ to SiC+ to SiC, 8.5−9.0 μm features become gradually weaker and the dust continuum becomes gradually redder, the type-Red sources have the reddest dust continuum and the type-Broad1 sources show a short-wavelength excess in the SiC dust feature. From Table 3, it is found that the dust type of group *A* is mainly SiC+ with a few cases of SiC++, and that of group *B* is mainly SiC with a few cases of SiC+. On the other hand, the SEDs of the objects of groups *C* and *D* (Fig. 2) show no obvious 8.5−9.0 μm emission features. Therefore, our classification seems to agree with Sloan's dust classification.

The relative integrated flux of the 11.30 μm SiC emission feature is compared with that of the absorption bands of HCN and C_2H_2 at around 3.05 and 13.70 μm in Figs. 12 and 13. Unexpectedly, no clear correlation is found in these two figures except several qualitative properties as follows: Group-*A* sources generally have relatively weaker 3.05 μm absorption and 11.30 μm emission but very strong 13.70 μm emission; objects in groups *B* and *C* are mixed together and so it is difficult to distinguish them by these three features alone.

3.1.5. The 13.70 μm C_2H_2 feature

In our samples, except IRAS 17419-1838, IRAS 12427+4542 and IRAS 22036+3315, all stars have the 13.7 μm C_2H_2 absorption feature. This suggests that the 13.70 μm feature is common in the spectra of carbon stars. Nevertheless, it is not clear why the three exceptional objects do not show this feature. Figure 14 shows the absorption features around 13.70 μm for typical objects from the four groups, and it can be seen that the absorption in the red wing of the profiles is generally stronger for objects from groups *A* and *D* than for objects from groups *B* and *C*. The correlation of the relative integrated flux with the normalized line center depth for this feature is shown in Fig. 15, where the different lines are obtained by linearly fitting the points of groups *A* and *D* respectively. One object in group *D*, IRAS 21027+5309, is far away from the other four objects in group *D*, and therefore this object has been excluded when fitting group-*D* data. Figure 15 shows that the 13.70 μm feature is particularly strong in group-*A* sources and most group-*D* sources but generally much weaker in the sources of groups *B* and *C*, except for the group-*B* object IRAS 21440+7324.

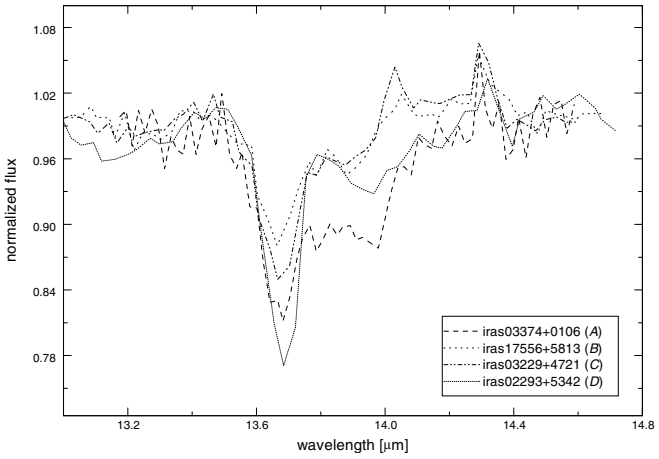

Fig. 14. Comparison of the typical 13.70 μm C_2H_2 absorption profiles from the four groups. The dashed line is for group-*A* object IRAS 03374+0106; the dotted line for group-*B* object IRAS 17556+5813; the dash-dot-dot line for group-*C* object IRAS 03229+4721; the short-dotted line for group-*D* object IRAS 02293+5342.

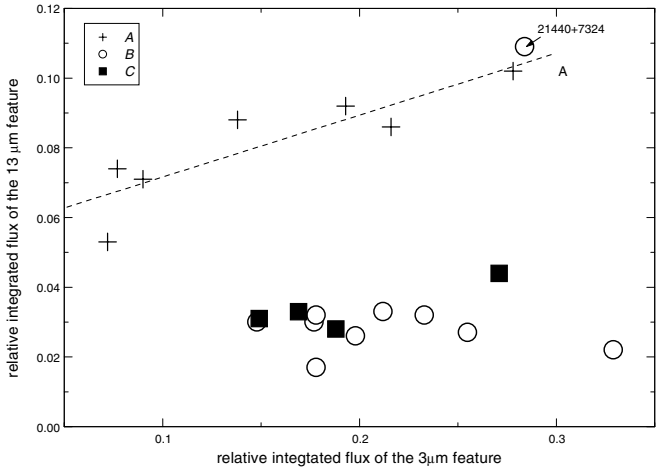

Fig. 15. Diagram of the relative integrated flux against the normalized line center depth for the 13.70 μm C_2H_2 feature. Group-*A* sources are represented by a cross; group-*B* sources by a circle; group-*C* sources by a square; group-*D* sources by a triangle. The different lines are derived by linearly fitting the points of groups *A* and *D* respectively. One object in group *D*, IRAS 21027+5309, has been excluded when fitting group *D*, because it is far away from the other four sources in group *D*.

If we consider the whole set of objects as a single group for Fig. 15, the correlation looks quite loose, although there seems to be a general trend. However, if we consider the objects in individual groups, the linear correlation becomes much better for groups *A* and *D* while group *B* still shows considerable scatter. This situation is similar to the one as we have addressed for the 11.30 μm SiC emission feature in Fig. 11. One object in group *D*, IRAS 21027+5309, is far away from the fitted line for group *D* but close to objects of groups *B* and *C*. The slope of the fitted lines increases from group *A* to *D*, in a similar manner as the slope of the fitted lines for the 11.30 μm feature increased from group *A* to *D* in Fig. 11. Line features with a similar line profile are expected to show a linear relation between the relative integrated flux and the normalized line center depth as shown here for individual groups; the difference of the line slopes may tell us that the basic profiles of the line feature are different for different groups. This variation of the basic line profiles of the 11.30 μm and 13.70 μm features, combined with the different quality of the linear fit of the points in different groups, has the following implications. On the one hand, the grouping based on the shape of the SED has successfully separated sources with different molecular features; on the other hand, the physical and chemical environment of groups *A*, *B*+*C* and *D* should be different. Probably, a difference in $T_{\rm eff}$ and in the radial distribution of the dust temperature in the envelope can influence the basic profile of the line features. However, without radiative transfer modelling, it is difficult to say which physical or chemical factors are responsible for the variation of the fitted linear relation slope.

Aoki et al. (1999) attributed the absorption feature at 13.70 μm to the C_2H_2 ν_5 bands. They found that this absorption feature is quite broad in the spectra of visual carbon stars. They pointed out that this broad absorption is due to not only the Q branches at 13.70 μm but also the P and R branches between 12 and 16 μm, and these features in the visual carbon stars are basically explained by absorption in the

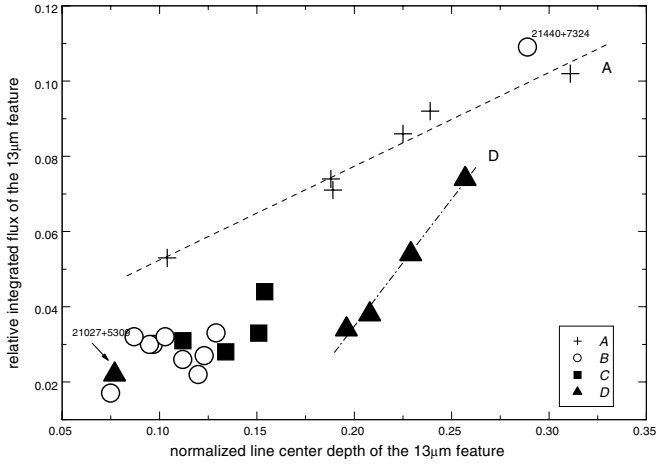

Fig. 16. Diagram of the relative integrated flux of the 13 μm C_2H_2 feature against that of the 3.05 μm C_2H_2+HCN feature. Group-*A* sources are represented by a cross; group-*B* sources by a circle; group-*C* sources by a square. The dashed line is derived by linearly fitting the points of group *A*.

photosphere or in the warm envelope close to the star. They also gave the absorption spectra of the C_2H_2 bands for temperatures of T = 1000 K and 500 K which are the temperatures of the background generating the 13.70 μm absorption feature, and remarked that the absorption bands of the P, Q and R branches are broader and stronger and the red wings of profiles of this feature are also stronger for higher temperatures. As shown in Fig. 14, group-*D* sources show a stronger red wing absorption for the 13.70 μm feature than group -*B* and *C* sources do, which may imply that the temperature of the inner envelope of sources from group *D* is higher than that from group -*B* and -*C* sources, because the 13.70 μm feature would be formed in the warm inner envelope (Aoki et al. 1999). However, $T_{\rm nir}$ of group *D* is

Table 4. SWS01 observational data and speeds of 17 carbon stars.

IRAS	*Name*	*Date*	*Speed*
$00172+4425$	$VX\ Aad$	$1997JAN17$	2
$01080+5327$	$HV\ Cas$	$1997AUG06$	1
$02270-2619$	$R\ For$	$1998FEB13$	1
$03229+4721$	$V384\ Per$	$1998FEB02$	2
$03374+6229$	$U\ Cam$	$1997AUG17$	2
$05028+0106$	$W\ Ori$	$1998MAR22$	3
$06226-0905$	$V636\ Mon$	$1998MAR31$	1
$12427+4542$	$Y\ CVn$	$1996APR25$	2
$12544+6615$	$RY\ Dra$	$1997MAY12$	3
$17419-1838$	$SZ\ Sgr$	$1998MAR28$	1
$18398-0220$	/	$1997MAR29$	2
$19068+0544$	/	$1997MAR09$	1
$19248+0658$	$V1421\ Aql$	$1998MAR22$	1
$21027+5309$	$V1899\ Cyg$	$1998JAN01$	1
$21358+7823$	$S\ Cep$	$1997MAY31$	1
$21440+7324$	$PQ\ Cep$	$1997JAN15$	1
$23257+1038$	$IZ\ Peg$	$1998JAN05$	1

For ISO SWS01 spectra, the models of different speeds (1, 2, 3, and 4) are corresponding to the different sepctral resolutions. The speed models 1, 2, 3, and 4 have respectively resolutions of about 400, 500, 800, 1500 at about 35 μm. The detail information about the resolutions of ISO SWS01 spectra can be referred to in ISO SWS Handbook.

lower than that of group *C*. A probable explanation is that for group *D* the circumstellar envelope is very thick while the $T_{\rm eff}$ of the center stars could begin to increase, which would cause the inner envelope to become warm.

In the 26 stars with 13.70 μm absorption, there are 19 objects with weaker emission at 14.30 μm, 6 of them also show very weak emission at 14.04 μm. From Table 3 we can see that the 14.30 μm weak emission commonly appears in most objects of the four groups while the 14.04 μm weak emission only appears in several objects of groups *B* and *C*. The absence of 14.04 μm emission in groups *A* and *D* may be due to its being buried in the strong red wing of the 13.70 μm absorption feature appearing in the two groups. Aoki et al. (1999) pointed out that the emissions at 14.04 and 14.30 μm are due to the HCN ν_2^1 and $2\nu_2^0$- ν_2^1 bands respectively. The excitation is due to radiative pumping of the HCN molecule from the ground level to the $2\nu_2^0$ level by 7 μm photons from the photosphere or from the inner envelope. Since these two HCN emission bands are detected in many of our samples, this means that HCN is quite common in carbon stars over a wide range of optical thickness of circumstellar envelopes, as mentioned by Aoki et al. (1999). However, the absence of these two HCN emission features in 10 of our samples does not necessarily imply that some carbon stars do not have HCN in their outer envelopes.

Both C_2H_2 and HCN show absorption features at both 3.05 and 13.70 μm, although the 13.70 μm absorption feature is mainly due to C_2H_2. The 3.05 μm feature and the 13.70 μm feature should show some kind of correlation. To determine the relationship among these four groups, we plot the relative integrated flux at 13.70 μm against that at 3.05 μm in Fig. 16 and fit the points of group *A* with a dashed line. In this figure, group-*A* sources are clearly separated from groups *B* and *C* while the latter two groups are mixed together. Group-*A* sources are fitted by the line quite well, while group -*B* and -*C* sources show 13.70 μm absorption with approximately the same relative integrated flux. This may indicate that, at least in sources of group *A*, the two features at 3.05 and 13.70 μm are varying in a similar manner. On the other hand, group-*A* sources generally show a much larger relative integrated flux in their 13.70 μm absorption feature than group -*B* and -*C* sources, and this tells us that C_2H_2 should have a much higher column density in the former than in the latter. However, this point has to be explained by detailed modelling. Note that group-*B* sources follow approximately the same linear relation as group-*C* sources, and this once again indicates that groups *B* and *C* have similar properties regarding the 13.70 μm feature. Noted also that, in all of our samples, the change of the relative integrated flux of the 13.70 μm feature is much smaller than that of the 3.05 μm feature. In addition, special attention should be given to group-*B* object IRAS 21440+7324, for it is far away from the majority of group-*B* sources but very close to the fitted line for group *A*. This object has been marked by its IRAS name in Fig. 15. Comparing the spectral shape and line strength of all 3.05, 5.20, 11.30 and 13.70 μm features of the object with those of the other objects, we find that this object is only similar to group-*A* sources in the 13.70 μm feature but much more similar to group-*B* sources in all other features. Thirdly, note a group-*B* object, IRAS 21358+7823, whose far-infrared continuum is found to fall much faster towards longer wavelengths than all other group-*B* sources (see Fig. 1), which may indicate that the contribution from the cooler dust for this object to the far-infrared continuum is less than in other group-*B* objects. Probably, the cooler part of the circumstellar envelope in this object is thinner than it is in the other objects in group *B*.

3.2. Additional discussion of group D

The five carbon stars in group *D* share two properties in their SEDs: (1) the infrared spectral flux is nearly zero in the near-infrared; (2) all of them show the double-peak feature. These two properties in common indicate that group-*D* sources have a cooler dust envelope than objects in the other groups. Two objects in group *D*, IRAS 02293+5748 and IRAS 21489+5301, were identified to be extreme carbon stars (Volk et al. 1992, 2000), while the types of the other three objects have not yet been identified. The main difference between the two extreme carbon objects and the other three is that the latter have relatively strong SiC emission. In addition, the relative integrated flux of the SiC feature of the latter three objects is close to that of group-*C* sources, while their SEDs are quite different. Considering the properties of SEDs and SiC dust emission for group-*D* sources, we suggest that group-*D* carbon stars are in the stage or pre-stage of extreme carbon stars. Another point is that two group-*D* objects (IRAS 02293+5748 and IRAS 21027+5309) have the very faint 3.05 μm absorption feature, which the others do not have.

4. Summary and conclusions

We have reduced and analyzed the ISO SWS spectra of 29 infrared carbon stars with an SiC feature at 11.30 μm, and

among them the ISO SWS spectra of 17 carbon stars not previously published. The absorption or emission features of molecules C_2, HCN, C_2H_2, C_3 and SiC are identified for the 17 unpublished carbon stars, and two unidentified absorption features at 3.50 μm and 3.65 μm are found for the first time. The 29 carbon stars are classified into groups *A*, *B*, *C*, and *D* according to the shapes of the ISO SWS spectra. Various aspects of the four groups are discussed and some conclusions are obtained:

1. Various groups in our classification directly reflect various stages on the evolutionary track of carbon stars. We suggest that the infrared spectra of carbon stars evolve along the sequence of *A*→*B*→*C*→*D*, during which $T_{\rm nir}$ decreases gradually and the circumstellar envelope gradually becomes thicker; at the same time, $T_{\rm eff}$ decreases gradually and the C/O ratio increases gradually from *A* to *B*. We found some features that vary in a regular manner from group *A* to *B* to *C* to *D*. On average, the relative integrated flux of the 3.05 μm HCN+C_2H_2 absorption feature increases gradually from group *A* to *B* and *C*; that of the 5.20 μm C_3 absorption becomes gradually weaker from group *A* to *B* and *C*; that of the 11.30 μm SiC emission increases gradually from group A to B and C but weakens in group *D*; and in contrast, that of the 13.70 μm C_2H_2 absorption is gradually weakened from group *A* to *B* and *C* but enhanced in group *D*.
2. For the classification, besides the evolutionary relation in the four groups (groups *A*, *B*, *C* and *D*), every group also has individual characteristics. Molecular absorption systems in the ISO of group *A* are quite different from those of group *B* and *C*, while the spectra of groups *B* and *C* have similar properties in many aspects and the spectra of group *D* are also again different from the former three groups. Firstly, the 3.05 μm absorption feature is narrower in group *A* than in groups *B* and *C*. Most group-*A* sources show two unidentified 3.50 and the 3.65 μm absorption features while no group -*B* and -*C* sources do. Moreover, none of the group-*A* shows the 3.9 μm C_2H_2 absorption (except IRAS 01246-3248) and the 3.56 μm HCN absorption, while these features appear in groups *B* and *C*. These differences between group *A* and groups *B*+*C*, are enough to indicate that group-*A* carbon stars have different properties from those in group *B* and *C*. Secondly, groups *B* and *C* look very similar in all aspects except line intensity, $T_{\rm eff}$ and $T_{\rm nir}$. Thirdly, the ISO SWS spectra of group *D* show an obvious double-peak feature, which indicates that group-*D* carbon stars are surrounded by a cooler dust envelope. However, as discussed above, fitting the physical quantities of the emission or absorption features with a linear function gives a more satisfactory result for groups *A* and *D* than for groups *B* and *C*; for an example, see the discussions about the 11.3 and 13.7 μm features (see Sects. 3.1.4 and 3.1.5).
3. Several other conclusions about the 5.20, 11.30 and 13.70 μm features are as follows.

   The shape of the 5.20 μm C_3 absorption feature does not vary essentially from group *A* to *B* and *C*; its intensity does vary. Its relative integrated line flux decreases with decreasing $T_{\rm eff}$ and $T_{\rm nir}$ along the *A*→*B*+*C* sequence and becomes undetectable in group-*D* sources. This declining tendency of the 5.20 μm feature can be explained directly by the decrease of the $T_{\rm eff}$ of the stellar photosphere and the increase of the optical depth in the circumstellar envelope along the same sequence. Because the condition for C_3 to form is, within strict limits, that the temperature should be around 2000 K, such a hot environment tends to disappear in the atmosphere of carbon stars from group *A* to *B*+*C*, and the increasing optical depth in the circumstellar envelope can weaken this absorption feature as well.

   Concerning the 11.30 μm SiC emission feature, it is stronger in groups *B* and *C* but weaker in groups *A* and *D*. This can be explained as an optical depth effect, i.e. the enhancement of the dust emission from *A* to *B*+*C* is due to the increase of dust content in their envelope, the opacity increasing significantly for group-*D* sources, for which only the outer and coolest layers of the circumstellar envelopes are detected. The actual peak wavelength varies among different sources in different groups. The SiC feature tends to peak at a shorter wavelength in sources of groups *B* and *C* than in sources of groups *A* and *D*. The profiles of the SiC feature are uniform for sources in one and the same group, and vary in a regular manner from group *A* to *B*+*C* to *D*.

   For the 13.70 μm C_2H_2 absorption feature, the red wing of profiles from sources of groups *A* and *D* has generally stronger absorption than does the red wing from sources in groups *B* and *C*, and the line center is especially deep in group-*A* sources and most group-*D* sources but generally much shallower in sources of groups *B* and *C*. Group-*D* sources show stronger red wing absorption than group -*B* and -*C* sources, which may imply that the temperature of the inner envelope of sources from group *D* is higher than that of the group -*B* and -*C* sources. However, $T_{\rm nir}$ of group *D* is lower than that of group *C*. A prossible explanation is that for group *D* the circumstellar envelope is very thick while the $T_{\rm eff}$ of central stars could begin to increase, which causes the inner envelope to become warm.

   For the 13.70 μm C_2H_2 absorption feature, there is another point to be noted. In 26 stars with 13.70 μm absorption, 19 show a weaker emission feature due to HCN at 14.30 μm, and 6 of 19 objects in addition show a very weak emission feature due to HCN at 14.04 μm. Also the 14.30 μm weak emission commonly appears in most sources of the four groups while the 14.04 μm weak emission only appears in several sources of groups *B* and *C*. The absence of 14.04 μm emission in groups *A* and *D* is thought to be due to its being buried in the strong red wing of the 13.70 μm absorption appearing in the two groups. On the other hand, some infrared carbon AGB stars have HCN emission features, indicating that the HCN molecule exists commonly in the outer circumstellar envelopes.

As our analysis only aims at infrared carbon stars with an SiC feature, the above conclusions should only be applicable to infrared carbon stars with such a feature.

Acknowledgements. We are grateful to Professor R. Szczerba for his help in the data processing. We are also grateful to the referee of this

paper for the suggests and comments on this paper. This work is supported by the NNSF of China (NO. 10073018) and the NSF of Yunnan province (NO. 2002A0021Q).

References

Aoki, W., Tsuji, T., & Ohnaka, K. 1998, A&A, 340, 222
Aoki, W., Tsuji, T., & Ohnaka, K. 1999, A&A, 350, 945
Bergeat, J., Knapik, A., & Rutily, B. 2001, A&A, 369, 178
Bryan, G., Volk, K., & Kwok, S. 1990, ApJ, 356, 301
Cernicharo, J., Goicoechea, J. R., & Caux, E. 2000, ApJ, 534, L199
Chan, S. J., & Kwok, S. 1988, ApJ, 334, 362
Chan, S. J., & Kwok, S. 1990, A&A, 237, 354
Chan, S. J. 1990, Ph.D. Thesis: The Evolution of carbon stars, P. 3, The universary of Calagry
Chen, P. S., Gao, H., Bao, M. X., & Chen, Y. K. 1990, in The Infrared Spectral Region of Stars, ed. C. Jaschek, & Y. Andrillat (Cambridge University Press), 385
Douglas, A. E. 1951, ApJ, 114, 466
Hron, J., Loidl, R., Kerschbaum, F., et al. 1997a, Ap&SS, 251, 211
Hron, J., Loidl, R., Kerschbaum, F., et al. 1997b, Ap&SS, 255, 359
Hron, J., Loidl, J., Höfner, S., et al. 1998, A&A, 335, L69
Iben, I. J., & Renzini, A. 1983, ARA&A, 21, 271
Jørgensen, U. G., Hron, J., & Loidl, R. 2000, A&A, 356, 253
Little-Marenin, I. R., & Little, S. J. 1988, ApJ, 333, 305
Loidl, R., Hron, J., Höfner, S., et al. 1997a, Ap&SS, 251, 243
Loidl, R., Hron, J., Aringer, B., et al. 1997b, Ap&SS, 255, L289
Loidl, R., Höfner, S., Jørgensen, U. G., et al. 1999, A&A, 342, 531
Kwok, S. 1993, ARA&A, 31, 63
Tsuji, T., Ohnaka, K., Aoki, W., et al. 1997, A&A, 320, L1
Sloan, G. C., Little-Marenin, I. R., & Price, R. D. 1998, ApJ, 115, 809
Volk, K., Kwok, S., & Langill, P. 1992, ApJ, 391, 285
Volk, K., Xiong, G., & Kwok, S. 2000, ApJ, 530, 408
Willems, F. J. 1988a, A&A, 203, 51
Willems, F. J. 1988b, A&A, 203, 65
Willems, F. J., & de Jong, T. 1988, A&A, 196, 173
Wood, P. R. 1985, in, Cools Stars with Excesses of Heavy Elements, ed. M. Jaschek, & P. C. Keenan (Reidel), 357
Yamamura, I., de Jong, T. D., Justtanont, K., et al. 1997, Ap&SS, 255, 351
Zuckerman, B., Gilra, D., Turner, B. E., et al. 1976, ApJ, 205, L15